Article

Synthesis of CSA-Capped Poly (Aniline-co-Aniline-2-Sulfonic Acid) Spherical Nanoparticles for Gas-Sensor Applications

Ki-Hyun Pyo , Ji-Sun Kim , Yoon Hee Jang , Jin-Yeol Kim *

Posted Date: 9 July 2025

doi: 10.20944/preprints202507.0811.v1

Keywords: acetone gas sensor; poly(aniline-co-aniline-2-sulfonic acid); room temperature; spherical nanoparticles

 doi:10.20944/preprints202507.0811.v1

Article

Synthesis of CSA-Capped Poly (Aniline-co-Aniline-2-Sulfonic Acid) Spherical Nanoparticles for Gas-Sensor Applications

Ki-Hyun Pyo [1], Ji-Sun Kim [1], Yoon Hee Jang [2] and Jin-Yeol Kim [1,*]

[1] School of Advanced Materials Engineering, Kookmin University, Seoul 02707, Korea

[2] Advanced Photovoltaics Research Center, KIST, Seoul 02792, Korea

* Correspondence: jinyeol@kookmin.ac.kr

Abstract

We synthesized emeraldine salts of poly(aniline-co-aniline-2-sulfonic acid) capped with camphorsulfonic acid (CSA), forming spherical nanoparticles (NPs), i.e., CSA-capped P(ANi-co-ASNi), and demonstrated their efficacy as gas sensor elements. The core-shell shaped spherical NPs exhibited an average diameter of 265 nm, with the hydrophobic CSA enabling chemical interactions with the outer surface of the positively charged P(ANi-co-ASNi) particles. These interactions facilitated stable charge transport within the copolymer chains while imparting resistance to external humidity. The synthesized CSA-capped P(ANi-co-ASNi) sensors reliably detected acetone gas at concentrations as low as 1 ppm and 1% RH water vapor at ambient temperature. These sensors also exhibited enhanced stability under various conditions, including variations in temperature, humidity, and cyclic performance, outperforming the conventional pure PANi.

Keywords: acetone gas sensor; poly(aniline-co-aniline-2-sulfonic acid); room temperature; spherical nanoparticles

1. Introduction

Polyaniline (PANi) is one of the most promising π-conjugated conductive polymers because of its re markable attributes, such as enhanced conductivity, robust environmental stability, ease of doping, and conductivity control, and a wide array of color changes corresponding to various oxidation levels [1–5]. PANi, known for its ability to dynamically and reversibly respond to environmental and external stimuli, has recently garnered significant attention. Moreover, its practical applications across various fields—including chemical sensors, optoelectronic devices, anticorrosion systems, and energy conversion technologies such as batteries and supercapacitors—have further elevated its prominence [6–10]. In particular, PANi-based electrochemical sensors have garnered considerable attention as highly promising materials for gas detection due to their dynamic resistance modulation when exposed to reducing or oxidizing harmful gases. Through chemical doping, charge carriers are introduced into the π-conjugated polymer backbone, influencing electrical conductivity. For instance, when a positively charged, doped PANi-based sensor is exposed to an oxidizing gas, its resistance increases in direct proportion to the concentration of the adsorbed gas. Conversely, upon adsorption of reducing components such as ammonia, the resistance also exhibits a measurable increase. Furthermore, PANi demonstrates intrinsic redox activity, as it facilitates the addition or removal of electrons within its π-conjugated polymer backbone through doping or de-doping processes involving dopants or oxidizing/reducing gaseous species. Regardless, PANi has been widely regarded as a highly promising material for chemical sensing applications, particularly in the detection of various organic gases such as ammonia (NH_3), acetone (C_3H_6O), carbon dioxide (CO_2), hydrogen (H_2),

 doi:10.20944/preprints202507.0811.v1

and gaseous H_2O [11–14]. Its electrical resistance undergoes significant modulation upon exposure to acidic or basic hazardous gases, making it an exceptionally responsive and adaptable sensing medium. PANi-based sensors possess several advantageous properties for gas detection, as demonstrated by numerous studies [15,16]. Nevertheless, overcoming several key challenges is essential to attaining the performance standards necessary for their effective deployment in real-world applications. Firstly, the sensor must demonstrate stable and efficient operation at ambient or low temperatures, ensuring precise detection of target gas species while minimizing cross-sensitivity to interfering compounds. Secondly, the advancement of sensing materials with exceptional resilience to humidity fluctuations is paramount to sustaining long-term operational reliability and accuracy. Thirdly, the sensor should exhibit superior selectivity for specific gaseous constituents, achieving highly sensitive detection capabilities even at concentrations as low as 1 ppm.

Many studies have been conducted on materials capable of achieving high sensitivity while ensuring moisture stability and maintaining detection at room temperature [17–20]. Zhang et al. [20] developed an acetone sensor using a ZnO/S-N graphite QD/PANi composite and reported a gas sensor capable of detecting 500 ppb at room temperature. Similarly, our research group previously developed an acetone gas sensor based on PANi nanoparticles (NPs) as part of an earlier study. However, the sensor has the challenge of achieving stable performance under variations in temperature, humidity, and repeated cycle evaluations [21]. To mitigate the aforementioned challenges, we designed spherical nanoparticles (NPs) composed of poly (aniline-co-aniline-2-sulfonic acid), capped with camphorsulfonic acid (CSA), herein referred to as CSA-capped P(ANi-co-ASNi), as shown in Figure 1. These engineered NPs have been specifically tailored for acetone gas sensing applications, ensuring enhanced sensitivity and selectivity. Structurally, it is a copolymer in which aniline monomer (ANi) and aniline-2-sulfonic acid monomer (ASNi) are used in equimolar amounts with a sulfonic acid ($-SO_3H$) group substituted at the 2-carbon position, and CSA is acted not only as a capping agent but also as a dopant. Specifically, PANi substituted with an $-SO_3H$ group is expressed as poly(aniline-2-sulfonic) (PASNi).

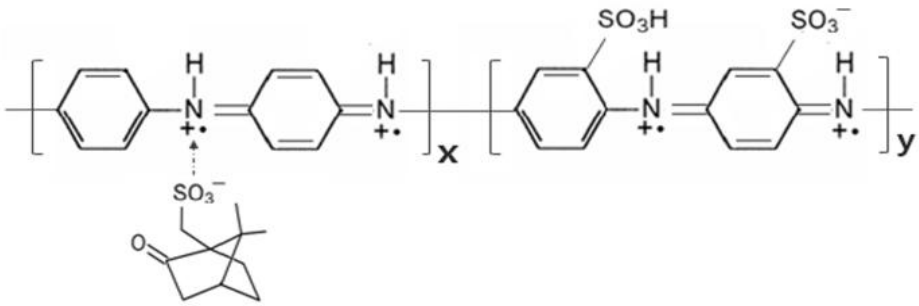

Figure 1. Schematic structure of poly (aniline-co-aniline-2-sulfonic acid) capped with CSA; CSA-capped P(ANi-co-ASNi). The molar ratio of x-to-y is 1:1.

In this study, we synthesized emeraldine salts of CSA-capped P(ANi-co-ASNi) in the form of core-shell shaped spherical NPs, specifically designed as sensing elements for acetone gas and gaseous H_2O (water vapor) detection. These engineered nanostructures aim to enhance sensitivity, selectivity, and stability in gas-sensing applications. Specifically, PANi substituted with an $-SO_3H$ group is expressed as poly(aniline-2-sulfonic) (PASNi). Here, the substituent $-SO_3H$ acts as a dopant, forming a self-doped conductive polymer. The $-SO_3H$ substituent directly donates electrons to the conjugated polymer chain, creating charged carriers and imparting conductivity. CSA with hydrophobic properties is positioned on the surface of P(ANi-co-ASNi) NPs. This configuration not only helps maintain a stable electrical resistance but can also minimize resistance changes due to humidity. Consequently, the CSA-

 doi:10.20944/preprints202507.0811.v1

capped P(ANi-co-ASNi) NPs were capable of reliably detecting acetone gas and H_2O vapor at concentrations of 1 ppm and 1% relative humidity (RH), respectively, at room temperature.

2. Experimental and Methods

2.1. Materials

Aniline (ANi, 99.0%), aniline-2-sulfonic acid (ASNi, 99.5%), hydroxypropyl methyl cellulose (HPMC), ammonium persulfate (APS, 98%), and camphorsulfonic acid (CSA) were purchased from Sigma-Aldrich (St. Louis, MO, USA). Hydrochloric acid (HCl, 35%) was obtained from Samchun (Seoul, Korea). High purity acetone gas with a concentration of 5 ppm was purchased from DK gas (Seoul, Korea).

2.2. Synthesis of CSA-Doped P(ANi-co-ASNi) Spherical Particles

CSA-capped P(ANi-co-ASNi) spherical NPs with a molar ratio of ANi-to-ASNi of 1:1 was synthesized via chemical oxidation polymerization, following the procedure illustrated in Scheme 1. First, 1.267 g of HPMC was dissolved in 20 ml of deionized (DI) water to prepare an aqueous dispersion, which was stirred sufficiently at room temperature for 30 min. This was referred to as solution A. Second, 200 μL of ANi and ASNi monomers (0.39 g) were introduced into a 50-mL flask and subjected to vigorous stirring at 50°C for 1 h to prepare a co-monomer solution, hereafter referred to as solution B. Upon the addition of solution B to solution A, the solution mixture was subjected to thorough stirring at 0°C–5°C for more than 30 min. Third, 4 mL of 1-M HCl was added to the solution mixture, and the resulting mixture was stirred for 10 min. Subsequently, a solution of APS (0.96 g) dissolved in 5 mL of DI water was gradually introduced dropwise. The reaction was then allowed to proceed without agitation at 0°C for 96 h. During the reaction, the product underwent a series of color changes: transitioning from dark yellow to blue within approximately 30 min, then to dark green after an additional 30 min, and ultimately stabilizing as green upon completion. The reaction product was isolated and purified by centrifugation. The spherical NPs obtained from the final step were redispersed in DI water (10 mL) to yield the desired suspension. Finally, 25 μL of a 1-M NaOH aqueous solution was carefully added dropwise to the previously dispersed P(ANi-co-ASNi) solution. The mixture was stirred at ambient temperature for 30 min, during which residual Cl^- ions from the synthesis were neutralized. Simultaneously, the positively charged PANi chains (emeraldine salts) underwent a transition to their neutral emeraldine base form. Subsequently, the purified products were redispersed in 10-mL DI water, followed by the addition of 50 μL of a 1-M CSA solution. The mixture was then agitated for more than 12 h. The purification process was performed as previously described, and redispersion was performed in a solvent such as water or alcohol. Ultimately, a dispersed solution comprising CSA-capped P(ANi-co-ASNi) spherical NPs was successfully obtained. CSA-capped P(ANi-co-ASNi) spherical NPs, with ANi-to-ASNi molar ratios of 0.8:0.2, 0.7:0.3, 0.6:0.4, and 0.5:0.5, were also synthesized by adjusting the amounts of ANi and ASNi monomers to match the respective molar ratios. All other conditions remained consistent with those previously described. CSA-capped P(ANi-co-ASNi) spherical particles with an ANi-to-ASNi molar ratio of 1:0, i.e., pure CSA-capped PANi, were also synthesized using only 400 μL of the ANi monomer.

 doi:10.20944/preprints202507.0811.v1

Scheme 1. Synthetic procedure for CSA-capped P(ANi-co-ASNi) spherical particles, along with their schematic structure and SEM image.

2.3. Measurements and Gas Detection Performance Evaluations

Initially, the prepared ink solutions of CSA-capped P(ANi-co-ASNi) spherical NPs were directly applied to a custom-made test substrate (test electrode cell: a silicon or polyimide (PI) substrate with a pair of gold interdigitated microelectrodes, maintaining an interelectrode distance of 0.5 mm) through drop-casting. Each microelectrode measured 1.5 ㎛ × 1 mm × 0.03 ㎛ (length × width × height) and exhibited an interelectrode gap of 0.5 mm. The coated substrate was subsequently dried in a vacuum oven at 80°C for 1 h under an inert atmosphere to facilitate solvent evaporation. Next, the CSA-capped P(ANi-co-ASNi) spherical particle sensor devices were installed within a gas chamber equipped with an electrical feed through and gas inlet and outlet ports. To ensure a dry and impurity-free environment, the chamber was purged with pure nitrogen (N_2) gas for 20 min before testing. Figure 2 presents the schematic representation of the sensor device and electrode architecture, which is based on CSA-capped P(ANi-co-ASNi) spherical particles.

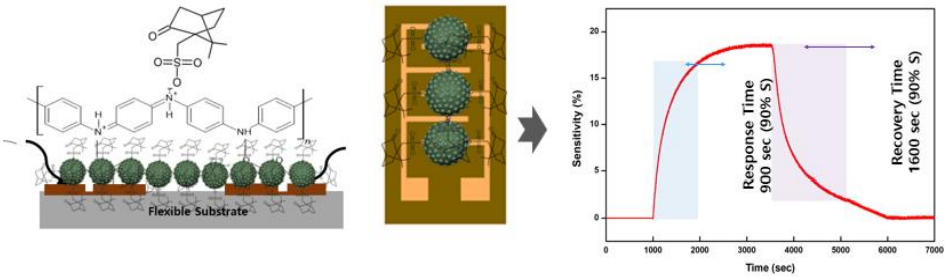

Figure 2. Schematic diagram of the sensor device and electrode based on the CSA-capped P(ANi-co-ASNi) spherical particles.

Acetone gas at concentrations of 1 to 5 ppm was generated by diluting 5 ppm acetone gas with dry air (0% RH) using a mass flow controller (MFC). The final concentration was controlled by adjusting the flow rate of 5 ppm acetone gas and dry air as follows: for 1 ppm, 40 sccm acetone and 160 sccm air; 2 ppm, 80 sccm acetone and 120 sccm air; 3 ppm, 120 sccm acetone and 80 sccm air; 4 ppm, 160 sccm acetone and 40 sccm air; and 5 ppm, 200 sccm acetone without dilution. All flows were regulated under standard temperature and pressure (STP). To supply water vapor at 100% relative humidity (RH), high-purity N_2 gas was bubbled through ultrapure water under STP conditions. The

 doi:10.20944/preprints202507.0811.v1

saturated vapor was delivered to the gas chamber at a constant flow rate of 2000 sccm. For experiments requiring lower humidity (1–5% RH), the saturated vapor (100% RH) was mixed with dry N_2 gas using MFCs to achieve the desired RH levels. The current resistance was measured in real time using a current-source meter (Keithley 2000, Keithley Co., Cleveland, OH, USA) by employing a DC voltage of 2 V under a room temperature. The morphology, microstructure, and electronic absorption of the CSA-capped P(ANi-co-ASNi) spherical particles were analyzed using scanning electron microscopy (SEM, JSM-633F, Jeol), Fourier transform Raman spectroscopy (Renishaw InVia Microscope, UK), and standard four-probe measurements (Loresta, Mitsubishi Chemical, Japan), respectively.

3. Results and Discussion

The overall synthesis procedure for CSA-capped P(ANi-co-ASNi) spherical NPs, using micelle polymerization with the HPMC surfactant in an aqueous solution, is depicted in Scheme 1. As shown in Scheme 1, the process began with dissolving HPMC, a surfactant essential for micelle formation, in DI water to prepare an aqueous solution. Subsequently, ANi and ASNi, substituted with a sulfonic acid (-SO_3H) group at the 2-carbon position, were added in equal molar amounts to the solution, and HCl was introduced into the previously prepared solution. During this step, the co-monomer comprising ANi and ASNi was protonated into positively charged anilinium ions (-NH_3^+) via HCl. In succession, the polymerization of the co-monomer was triggered by the addition of APS, as an oxidizing agent. Afterwards, the impure ion products were neutralized and eliminated using NaOH solution, resulting in the spherical NPs of blue-colored emeraldine base structure. Finally, CSA was used for re-doping, resulting in a green-colored emeraldine salts structure-based electrically conductive NPs, as showed in the Scheme 1. As depicted in the Scheme 1, this process yielded green P(ANi-co-ASNi) spherical NPs capped with CSA. Here, the spherical NPs exhibited an average diameter of 265 nm, with the hydrophobic CSA chemically bonded to the outer surface of the positively charged P(ANi-co-ASNi) spherical NPs. In this context, the CSA capping agent, featuring an -SO_3H functional group, promotes stable charge transfer properties within the P(ANi-co-ASNi) polymer chains while enhancing the resistance of the structure to external moisture. In addition, the CSA-capped P(ANi-co-ASNi) NPs exhibit the properties of p-type semiconductors, which are characterized by positively charged chain structures. The NH^+ functional group within the P(ANi-co-ASNi) polymer chain can form weak hydrogen bonds with C=O or H^+/OH via charge-charge interactions when acetone or H_2O molecules are adsorbed. This means that when the C=O group of acetone molecule is adsorbed, the positive charge density within the backbone of P(ANi-co-ASNi) decreases, thereby increasing the electrical resistance. Conversely, upon adsorption of H_2O molecules, the positive charge density along the P(ANi-co-ASNi) backbone increases. When H_2O acts as a charge acceptor, this interaction further reduces the net positive charge, resulting in decreased electrical resistance. Previous studies have reported on the reaction mechanisms between PANi-based materials and various organic gases [22,23]. Moreover, the spherical morphology of CSA-capped P(ANi-co-ASNi) particles provides a high surface-to-volume ratio, which significantly enhances the interaction between the polymer chains and gaseous analytes.

Figure 3 shows the SEM images of the as-synthesized P(Ani-co-ASNi) NPs prior to capping and the P(Ani-co-ASNi) NPs after CSA capping. As illustrated in the figure, the particles of P(Ani-co-ASNi) and CSA-doped P(Ani-co-ASNi) consist of well-ordered spherical NPs, with average diameters of approximately 235 and 265 nm, respectively. The diameter of CSA-capped P(Ani-co-ASNi), which was produced by secondary capping with CSA, is approximately 30 nm larger than that of P(Ani-co-ASNi). These results suggest that CSA is enveloped on the P(Ani-co-ASNi) surface, with an estimated thickness of approximately 30 nm. The electrical resistance of the as-prepared P(Ani-co-ASNi) NPs was measured to be approximately 1.2 MΩ, whereas upon capping with CSA to form a thickness of about 30 nm,

 doi:10.20944/preprints202507.0811.v1

the resistance decreased to approximately 0.6–0.8 MΩ. The observed decrease in electrical resistivity is attributed to the partial doping effect of camphorsulfonic acid (CSA), which incorporates a sulfonic acid group as a substituent. CSA functions not only as a capping agent but also serves as a dopant, thereby contributing to enhanced electrical properties. These findings suggest that CSA plays a dual role, acting simultaneously as a surface modifier and a chemical dopant. In addition, energy-dispersive X-ray spectroscopy (EDS) spectra were analyzed to determine the elemental composition of the NPs (Figure 3, I-a and II-a). In this study, a thin CSA layer containing a -SO_3H functional group uniformly coated the entire surface of the P(ANi-co-ASNi) particles. Consequently, the mass percentage of sulfur (S) atoms in CSA-capped P(Ani-co-ASNi) was quantified and compared with the proportions of other constituents. The results of the analysis (Figure 3 (II-a)) show that the mass percentage of S atoms in the CSA-capped P(Ani-co-ASNi) particles is 3.13%. In contrast, the EDS spectrum of P(Ani-co-ASNi) particles without CSA (Figure 3 (I-a)) reveals only a small quantity of S atoms, amounting to 0.63%. The presence of these S atoms in the P(Ani-co-ASNi) particles is attributed to the -SO_3H group, which acts as a substitutent in PASNi, a copolymer of PANi. Ultraviolet/visible/near-infrared (UV/Vis/NIR) spectroscopy and Raman spectroscopy were used to examine changes in the charge transport properties and molecular structure of the CSA-capped P(ANi-co-ASNi) copolymer (Figure 4). Figure 4-(I) shows the UV/Vis absorption spectra, highlighting the spectral changes corresponding to the molar ratios of ANi and ASNi in the P(ANi-co-ASNi) copolymer. Figure 4-I-(a) shows the UV/Vis absorption spectra of the P(ANi-co-ASNi) sample with an Ani-to-ASNi molar ratio of 1:0, representing the spectrum of pure PANi. Three characteristic absorption peaks are observed at 354, 440, and 883 nm. Here, the peaks at 354 and 440 nm are attributed to the π–π* excitation of the *para*-substituted benzenoid segment (-benzene-NH-benzene-). In contrast, the peak at 883 nm corresponds to the π–π* excitation of the quinoid structure (-N=quinone=N-) [24,25].

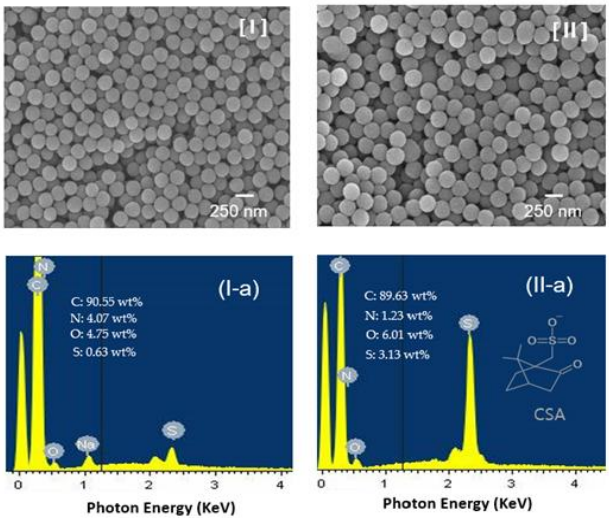

Figure 3. (I) SEM images of P(ANi-co-ASNi) sample before doping and (II) CSA-capped P(ANi-co-ASNi) sample after CSA capping. (I-a) and (II-a) show the EDS spectra and corresponding elemental analysis data for each sample.

However, as shown in Figures 4-I-(b), (c), and (d), when the Ani-to-ASNi molar ratio was adjusted to 0.8:0.2, 0.7:0.3, and 0.6:0.4, respectively, the absorbance intensity of the peaks at 440 and 883 nm exhibited a decreasing trend. This phenomenon is attributed to the weakening of the quinoid structure in ANi as the proportion of ASNi increases. However, when the ANi-to-ASNi molar ratio in CSA-capped P(ANi-co-ASNi) was 0.5:0.5, a new UV/Vis absorption peak emerged (Figure 4-I-(e)). Specifically, a new absorption peak emerged at 312 nm, and the peak at 883 nm shifted to 905 nm, extending into the near infrared (NIR) region. In contrast,

 doi:10.20944/preprints202507.0811.v1

no notable changes were detected in the peaks at 354 and 440 nm. The peak at 312 nm appears to be due to self-doping induced by the quinonoid region, which forms when the sulfonic acid group of ASNi donates electrons to the PASNi chain. In the CSA-capped P(ANi-co-ASNi) structure with an ANi-to-ASNi molar ratio of 0.5:0.5, the sulfonic acid ion of CSA is believed to interact with P(ANi-co-ASNi) via the π-conjugated chain, resulting in protonation at the imine nitrogen sites. This interaction promotes the formation of a π-conjugated system with delocalized electrons, thereby enhancing electrical conductivity. Experimentally, the electrical resistance of pristine P(ANi-co-ASNi) was measured to be approximately 1.2 MΩ, whereas that of CSA-capped P(ANi-co-ASNi) was reduced to 0.6–0.8 MΩ, indicating a resistance decrease of over 30%.

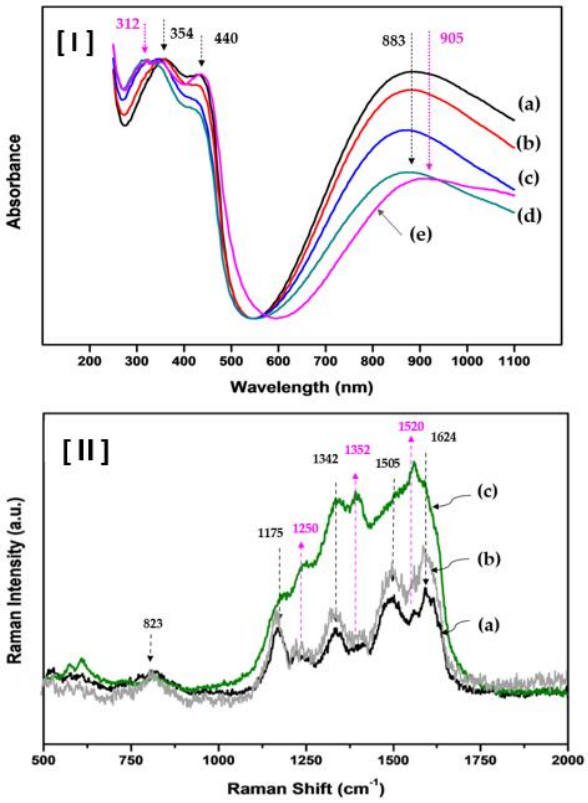

Figure 4. (I) UV/vis absorption spectra of CSA-capped P(ANi-co-ASNi) samples with various Ani-to-ASNi molar ratios in P(ANi-co-ASNi) copolymers: (a) 1:0, (b) 0.8:0.2, (c) 0.7:0.3, (d) 0.6:0.4, and (e) 0.5:0.5. (II) Raman spectra of CSA-capped P(ANi-co-ASNi) samples with various Ani-to-ASNi molar ratios: (a) 1:0, (b) 0.8:0.2, and (c) 0.5:0.5, respectively.

Raman spectroscopy was performed to investigate the chemical bonding structures and their influence on the charge transport mechanism in CSA-capped P(ANi-co-ASNi) (Figure 4 (II)). Figure 4-II-(a) shows the Raman spectrum of the P(ANi-co-ASNi) sample with an ANi-to-ASNi molar ratio of 1:0, representing the Raman spectrum of pure PANi. The band at 823 cm^{-1} is attributed to the C–H out-of-plane vibration in the 1,4-distributed benzene ring. Peaks corresponding to the bending modes of the benzene ring, the C–N stretching of the aromatic ring, and the stretching of the charged C–NH^+ group were observed between 1250 and 1352 cm^{-1}. The bands at 1175 cm^{-1} are assigned to the -SO_3H group associated with CSA. In addition, peaks for the C=C stretching of the quinoid structure (-N=quinone=N-) are observed at 1624 cm^{-1}, whereas the bands at 1505 cm^{-1} are attributed to the C=C stretching of the benzoid structure (-N=benzene=N-) [26–29]. Finally, the intensity ratio of the bands at 1624 cm^{-1} and 1505 cm^{-1} reflects the conjugation length and doping level of the PANi chain. Typically, longer conjugation lengths and higher doping levels result in a more pronounced intensity of the

 doi:10.20944/preprints202507.0811.v1

1624 cm^{-1} peak compared to the 1505 cm^{-1} peak [30]. Figures 4-II-(b) and (c) show the Raman spectral characteristics of the copolymers synthesized with Ani-to-ASNi molar ratios of 0.8:0.2 and 0.5:0.5, respectively. As the ASNi content increased, a marked enhancement in the intensities of the peaks at 1250, 1352, and 1520 cm^{-1} was observed. In addition, the Raman absorbance in the range of 1175 and 1624 cm^{-1} was significantly stronger than that of pure PANi (Figure 4-II-(a)). Accordingly, the peak at 1250 cm^{-1} in CSA-capped P(ANi-co-ASNi) is attributed to the -SO_3H substitution group within the ASNi structure. The peak at 1352 cm^{-1} corresponds to the stretching mode of the charged C–NH^+ group within the quinoid structure of PASNi, and the peak at 1520 cm^{-1} corresponds to the C=C/C–C stretching mode of the benzoid structure of PASNi.

Acetone gas, found in trace amounts of less than 1 ppm in human exhaled breath, is associated with metabolism and has been used as a medical biomarker for diabetes [31–33]. Therefore, it is essential to accurately detect acetone gas concentrations in the range of tens of ppb emitted during respiration. In this study, we developed an acetone gas sensor by drop-casting an ink solution comprising CSA-capped P(ANi-co-ASNi) onto a sensor substrate integrated with a pair of gold electrodes. The test cell consists of a pair of gold electrodes embedded on a Si substrate, serving as the sensor. Acetone gas concentrations of up to 1 ppm and gaseous H_2O levels of up to 1% RH were stably detected using the developed sensor at room temperature. The real-time responses of the CSA-capped P(ANi-co-ASNi) sample were systematically measured to evaluate their sensing capabilities for acetone and H_2O vapor (Figure 5). The sensor's performance was evaluated under various conditions, including repeated recovery characteristics, fluctuations in temperature, humidity, and gas flow rates (Figure 6). Figure 5-(I) shows the continuous dynamic response of the CSA-capped P(ANi-co-ASNi) sensors to acetone gas concentrations ranging from 1 to 5 ppm, maintained at a constant temperature of 25°C and 0% RH. Figures 5-(I-a) and 5-(I-b) show the sensor performance of the CSA-capped P(ANi-co-ASNi) copolymers, with ANi-to-ASNi molar ratios of 1:0 and 0.5:0.5, respectively. The responsiveness (S%) of the CSA-capped P(ANi-co-ASNi)-based sensors to acetone gas was measured in real-time using the normalized change in resistance, $\Delta R/R_i = (R_i - R_0)/R_i \times 100$. Here, Ri denotes the initial resistance before gas exposure, R_0 denotes the real-time resistance during gas exposure, and ΔR represents the difference between Ri and R_0, which is calculated after gas exposure. Figure 5-(I-a) shows the continuous dynamic response of a CSA-capped P(ANi-co-ASNi) sample with an ANi-to-ASNi molar ratio of 1:0, corresponding to pure PANi, during its exposure to acetone gas. The effective S value was measured for each acetone gas concentration (1, 2, 3, 4, and 5 ppm), with the S value at 1 ppm determined to be 4.2 (absolute value). In addition, this S value showed that an increase in the gas concentration corresponded to a proportional decrease in relative reactivity in the negative (-) direction. This negative shift in the S value is attributed to the decreased charge density of the PANi backbone caused by the adsorption of acetone gas. The increased electrical resistance observed during the process can be attributed to the interaction between acetone gas molecules and the amine nitrogen (–NH^+) sites present in the backbone of the PANi polymer. This indicates that hydrogen bonds (O–H) are formed between the NH^+ sites of PANi and the oxygen (O) atoms in acetone molecules. These newly formed O–H bonds interfere with charge transfer in the PANi chains, causing a negative shift in the S value of the PANi structures. This observation suggests that hydrogen bonding significantly influences the electronic properties of the PANi polymer, particularly charge transport in the PANi backbone. Figure 5-(I-b) shows the continuous dynamic response of the CSA-capped P(ANi-co-ASNi) copolymers synthesized with equal ANi-to-ASNi molar ratio. The S value for acetone gas in these copolymer samples exhibited a significant reduction compared to that of pure PANi (Figure 5-(I-a). At 1 ppm, the S value was 1.9 (in absolute terms), reflecting the diminished sensitivity under these specific conditions. Despite the marked decrease in responsiveness compared to pure PANi, the CSA-capped P(ANi-co-ASNi)-based sensor

 doi:10.20944/preprints202507.0811.v1

showed consistent reactivity and excellent reproducibility to acetone gas. In the P(ANi-co-ASNi) copolymer, PASNi represents PANi substituted with an SO_3H group. The incorporation of the SO_3H substituent serves as an intrinsic dopant, effectively transforming the material into a self-doped conductive polymer while ensuring stable electrical conductivity. However, as shown in Figure 5-(I-b), the sensitivity of the copolymer was relatively stable, exhibiting consistent proportional changes with respect to the acetone gas concentration. This stability highlights the reliability of the copolymer in effectively detecting gas at various concentrations. The response time refers to the interval required for the conductance of a sensor to achieve 90% of its maximum (saturated) response signal, as shown in Figure 2. Conversely, the recovery time is the duration required for a sensor to return to a conductance level that is 10% above its baseline value when exposed to air. These metrics are crucial for evaluating the efficiency and reliability of sensor performance under dynamic conditions. The CSA-capped P(ANi-co-ASNi)-based sensors, with ANi-to-ASNi molar ratios of 1:0 and 0.5:0.5, exhibited response times of 1,200 and 1,700 s, respectively, when subjected to 1-ppm acetone gas at 25°C and 0% RH. Furthermore, their recovery times were measured at 1,500 and 2,700 s, respectively. In particular, as depicted in the figure 4, the recovery time exhibited a significant increase with increasing reacting gas concentration. This prolongation can be ascribed to the extended desorption process at room temperature, which becomes more time-intensive as the amount of gas adsorbed increases. Interestingly, this effect was more prominent in the copolymer bound to PASNi than in pure PANi, highlighting the distinct desorption dynamics influenced by the structural differences between the materials.

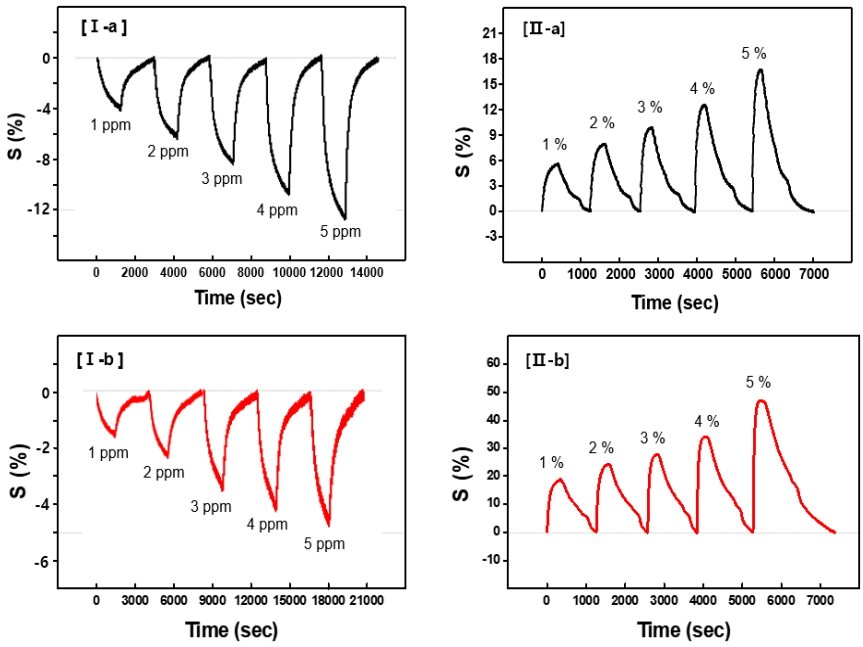

Figure 5. Continuous dynamic response of CSA-capped P(ANi-co-ASNi) NP-based sensors to various concentrations of [1] acetone gas ranging from 1 to 5 ppm and [II] gaseous H_2O ranging from 1 to 5 % at 25°C and 0% RH. The Ani-to-ASNi molar ratio of the P(ANi-co-ASNi) copolymers are as follows: (a) 1:0 and (b) 0.5:0.5.

Figure 5-(II) shows the continuous dynamic response (S) of the CSA-capped P(ANi-co-ASNi) sensors exposed to gaseous H_2O concentrations ranging from 1 to 5% RH. The S value for the CSA-doped pure PANi sample was approximately 5.8 when exposed to 1% RH H_2O vapor (Figure 5-(II-a)). This result reflects the high S value of the sensor to low H_2O vapor concentrations under the specified conditions. Unlike acetone gas, H_2O vapor exhibited a distinctive trait in which the responsive value increased proportionally in the positive (+) direction as the concentration increased. Here, H_2O vapor is thought to function as an acid, interacting with CSA-doped pure PANi chains to reduce their electrical resistance. This effect

 doi:10.20944/preprints202507.0811.v1

aligns with the properties of p-type semiconductors, where charge carriers (holes) are positively influenced, enhancing conductivity. As shown in Figure 5-(II-b), the S value of the CSA-capped P(ANi-co-ASNi) copolymer samples increased by approximately four times that of pure PANi. This remarkable improvement appears to be primarily driven by the significant contribution of ASNi, which substantially enhances the reactivity of the copolymer toward H_2O vapor.

Figure 6 shows that the sensors exhibit a linear response, where the S value consistently increase with increasing concentration of the injected gas. This linearity highlights the reliability and accuracy of the sensors detecting various gas concentrations, highlighting their potential for precise quantitative analysis. Based on these results, the slope of the S value vs. acetone gas concentration was analyzed, leading to the determination of sensitivity in units of ppm^{-1}. The acetone sensors based on pure PANi and the P(ANi-co-ASNi) copolymer exhibited sensitivity values of 2.13 and 0.84, respectively (Figure 6-(I)). The H_2O vapor sensor exhibited significantly higher sensitivity (2.69) than the acetone sensor (6.65) (Figure 6-(II)). All experimental data were acquired from a minimum of five repeated measurements conducted under identical environmental conditions, and the averaged values were utilized for analytical evaluation. To ensure precision and reliability, data falling within the measurement error range were excluded from the final analysis. However, the CSA-capped P(ANi-co-ASNi)-based sensor exhibited a remarkable sensitivity value of 6.65 to H_2O molecules. This result can be attributed to the hydrophilic nature of the $-SO_3H$ substitution group in PANi, which promotes the adsorption of H_2O molecules. In addition, the presence of the $-SO_3H$ group creates favorable conditions for interactions with H_2O molecules, enhancing the reactivity and sensitivity of the sensor to H_2O vapor.

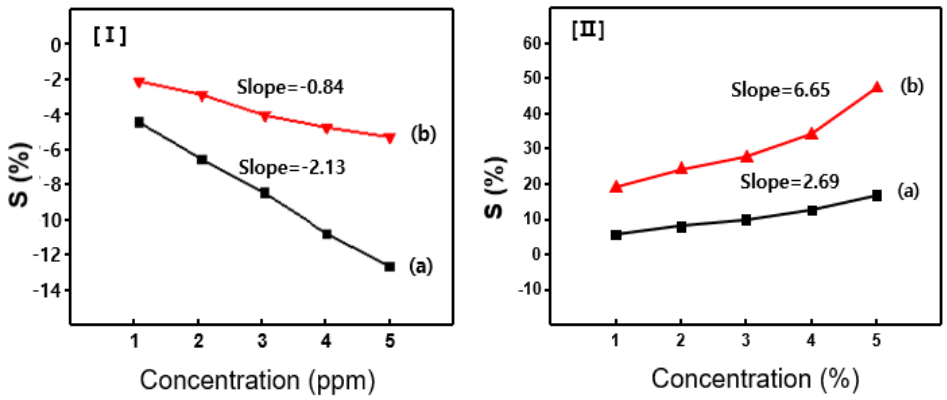

Figure 6. Calibration curves showing the variations in sensitivity of CSA-capped P(ANi-co-ASNi) NP-based sensors in response to [I] acetone and [II] H_2O vapor concentrations. The Ani-to-ASNi molar ratio of the P(ANi-co-ASNi) copolymers are as follows: (a) 1:0 and (b) 0.5:0.5.

Figure 7-(I) shows the results of the reliability verification experiments in which cyclic testing was conducted on the acetone sensor samples based on CSA-capped P(ANi-co-ASNi). These experiments aimed to evaluate the performance consistency and stability of the sensor under repeated exposure to acetone gas, providing insights into its durability and long-term reliability. These experiments were conducted under rigorously controlled conditions, including 25°C, 0% RH, and an acetone gas concentration of 1 ppm. This approach ensured consistency in the experiment environment, enabling a thorough assessment of the sensor performance over repeated cycles. As shown in Figure 7-(I-a), the PANi-based sensor exhibited a ΔS value exceeding 11% during the 10-cycle test at an acetone gas concentration of 1 ppm. In contrast, as shown in Figure 7-(I-b), the P(ANi-co-ASNi)-based sensor exhibits a more moderate change in ΔS (approximately 5%–6%) while maintaining a relatively high recovery rate. Figures 7-(II), (III), and (IV) show the performance of the sensor under various

 doi:10.20944/preprints202507.0811.v1

external environmental factors such as temperature, RH, and gas pressure. The changes in performance were carefully tracked by monitoring variations in the electrical resistance of the sensor cell. Figure 7-(II-a) illustrates the impact of temperature on the performance of the PANi-based sensor. As the external temperature increased to 125°C, the electrical resistance changed, increasing by approximately 40% in the positive (+) direction. In contrast, for the CSA-capped P(ANi-co-ASNi)-based sensor (Figure 7-(II-b)), a proportional decrease in its electrical resistance of approximately 40% was observed under the same conditions. These results indicate that in CSA-capped PANi sensors, electrical resistance decreases as temperature rises. In contrast, CSA-capped P(ANi-co-ASNi)-based sensors exhibit an inverse behavior, with resistance increasing as the temperature elevates. This highlights the differing sensitivity dynamics between the pure PANi doped with CSA and CSA-capped P(ANi-co-ASNi)-based sensors at different temperature. Figure 6-(III) shows the variations in the electrical resistance of the sensor as it responds to various RH levels ranging from 0% to 87%.

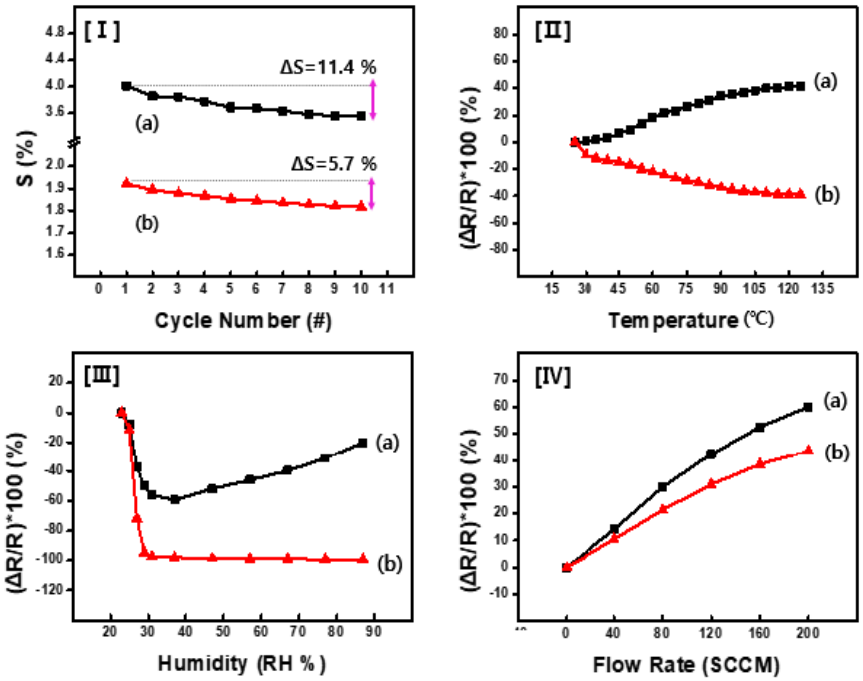

Figure 7. [I] Changes in responsiveness (S%) at acetone gas concentration of 1 ppm as a function of the number of repetitions at 25°C and 0% RH. [II] Variation in electrical resistance corresponding to temperature changes between 25°C and 125°C at 0% RH. [III] Variations in electrical resistance with respect to humidity levels ranging from 0% to 87% RH. [IV] Variations in electrical resistance as a function of gas flow rates ranging from 0 to 200 sccm under dry conditions. The ANi-to-ASNi molar ratio of the P(ANi-co-ASNi) copolymers are as follows: (a) 1:0 and (b) 0.5:0.5.

It is widely recognized that acetone gas sensors are particularly susceptible to ambient humidity. As shown in Figure 7-(III), an interesting trend was observed in this study: all tested sensors exhibited a proportional decrease in electrical resistance as the relative humidity (RH) increased up to 28% RH. Beyond this threshold, however, the sensors displayed a non-linear and divergent response pattern. This suggests that under low humidity conditions (<28% RH), the interaction between acetone molecules and the PANi backbone is enhanced—likely due to the absence of significant moisture interference, resulting in improved charge transfer. In contrast, at higher humidity levels (>28% RH), the adsorption of acetone appears to be hindered by increasing amounts of water vapor. This suggests that under low humidity conditions (<28% RH), the interaction between acetone molecules and the PANi backbone is

 doi:10.20944/preprints202507.0811.v1

enhanced—likely due to the absence of significant moisture interference, resulting in improved charge transfer. In contrast, at higher humidity levels (>28% RH), the adsorption of acetone appears to be hindered by increasing amounts of water vapor. Prior literature [34,35] supports this behavior, indicating that acetone molecules form hydrogen bonds with water vapor—particularly via interactions between the carbonyl oxygen of acetone and the hydroxyl (-OH) groups in water molecule—leading to a reduced availability of acetone for binding with the PANi backbone. Under identical test conditions, the CSA-capped P(ANi-co-ASNi) sensor (Figure 7-(III-b)) showed minimal variation in resistance even above 28% RH, with a relative change below 5%. This stability is attributed to the bulky sulfonic acid (-SO_3H) groups on the ASNi units, which contribute to a sterically hindered surface structure that resists water condensation and limits moisture-related interference. These observations suggest that at RH levels beyond 28%, acetone adsorption approaches saturation due to competition with water vapor. This behavior may provide an opportunity for stable signal output in humid environments. We also speculate that saturation humidity could shift with temperature; however, such effects were beyond the scope of this study and require further investigation in future work. As shown in Figure 7-(IV), the P(ANi-co-ASNi)-based sensor exhibited approximately 15% lower pressure resistance to gas flow compared to the pure PANi-based counterpart. This discrepancy underscores distinct structural and compositional differences that significantly influence the performance of the two sensors under varying pressure conditions.

Selectivity is a key parameter in the practical application of gas sensors. To evaluate selectivity, responsiveness to various organic gases, including ethanol, methanol, chloroform, xylene, toluene, cyclohexane, and hydrogen, was investigated. According to the previous results, the CSA-capped P(ANi-co-ASNi) sensor with an ANi-to-ASNi molar ratio of 0.5:0.5 exhibited an S value of –5.2 for 5-ppm acetone gas and +20 for 1% H_2O gas. The sensor also exhibited a response (S= –12 at 5ppm) to ethanol and methanol gases but negligible responses, even at a high concentration of 5 ppm, to other gases such as xylene, toluene, cyclohexane, and hydrogen. Interestingly, the sensor exhibited negative responsiveness to gases acetone and alcohols, which possess acidic properties, because of a decrease in the electrical resistance of the sensor. Conversely, the sensor exhibited positive responsiveness to gases with basic properties, such as chloroform, toluene, xylene, and cyclohexane.

4. Conclusions

In this study, we systematically designed and synthesized a CSA-capped P(ANi-co-ASNi) NPs-based acetone gas sensing material, integrating spherical NPs to optimize detection efficiency. The sensor's performance was evaluated across acetone gas concentrations ranging from 1 to 5 ppm under ambient conditions, demonstrating exceptional sensitivity and strong potential for practical applications in precise gas detection. Additionally, the sensor exhibited effective responsiveness to gaseous H_2O, achieving reliable detection even at concentrations as low as 1%. The spherical NPs exhibited an average diameter of 265 nm, with the hydrophobic CSA capping agent capable of chemically interacting with the outer surface of the positively charged P(ANi-co-ASNi) NPs. These structural characteristics could contribute to enhanced stability under high humidity conditions, ensuring reliable sensor performance. The structural properties of the newly synthesized sensing material were systematically investigated through SEM, TEM, EDS, EUV, and Raman spectroscopic analyses. These comprehensive characterizations enabled an in-depth elucidation of the sensing mechanism, offering valuable insights into its functional attributes and gas detection pathways. Ultimately, the developed sensors demonstrated enhanced stability across diverse environmental conditions, including fluctuations in temperature, humidity, gas flow rates, and cyclic performance. These advancements significantly surpassed the performance of conventional pure PANi-based sensors, highlighting their potential for reliable and precise gas detection in practical applications.

 doi:10.20944/preprints202507.0811.v1

Author contributions: Ki-Hyun Pyo: Writing-original draft, visualization, validation, methodology, material synthesis experiments, and data analysis and supported the writing of the manuscript. Ji-Sun Kim: Validation, formal analysis, data curation, material synthesis experiments and data analysis. Yoon Hee Jang: Participated in validation, formal analysis, data analysis curation, and Raman spectroscopy experiments and data interpretation. Jin-Yeol Kim: Writing-original draft, supervision, grant acquisition, conceptualization, visualization, validation, methodology, data analysis, and wrote the manuscript.

Funding: This work was financially supported by National Research Foundation of Korea (NRF) grant funded by the Korea government (Ministry of science and ICT: MIST) (2021R1F1A1105389111).

Data availability: Data will be made available on request

Conflicts of interest: The authors declare that there are no conflicts of interest in the results and content of the study.

References

1. Verma, A.; Kumar, T., PANI@Ag nanocomposites gas sensors for rapid detection of ammonia, *Polyhedron*, **2024**, 116982.
2. Jang, J.S.; Ha, J.S.; Cho, J.H., Fabrication of water dispersible polyaniline-poly(4-styrenesulfonate) nanoparticles for inkjet-printed chemical sensor applications, *Adv. Mater.*, **2007**, 19, 1772–1775.
3. Verma, A.; Kumar, T., Gas sensing properties of a Cu-doped PANI nanocomposite towards ammonia, *Mater. Adv.*, **2024**, 5, 7387-7400.
4. Varela-Alvarez, A.; Sordo, J.A.; Scuseria, G.E., Doping of Polyaniline by Acid−Base Chemistry: Density Functional Calculations with Periodic Boundary Conditions, *J. Am. Chem. Soc.*, **2005**, 127, 11318.
5. Kim, J.S.; Byeon, J.H.; Kang, S.M.; Kim, J.Y., A high sensitivity acetone gas sensor based on polyaniline–hydroxypropyl methyl cellulose core–shell-shaped nanoparticles, *Nanoscale Adv.*, **2022**, 4, 5312–5319.
6. Zhang, Z.; Sui, J.; Zhang, L.; Wan, M.; Wei, Y.; Yu, L., Hollow Micro-/Nanostructures: Synthesis and Applications, *Adv. Mater.*, **2005**, 17, 2854.
7. Kroutil, J.; Laposa, A.; Povolny, V.; Klimsa, L.; Husak, M. Gas Sensor with Different Morphology of PANI Layer *Sensors*, **2023**, 23, 1106 (1-14).
8. He, X.; Yang, W.; Mao, X.; Xu, L.; Zhou, Y.; Chen, Y.; Zhao, Y.; Yang, Y.; Xu, J., *J. Power Sources*, **2018**, 376, 138–146.
9. Moon, S.; Jung, Y. H.; Kim, D. K., Enhanced electrochemical performance of a cross-linked polyaniline-coated graphene oxide-sulfur composite for rechargeable lithium–sulfur batteries, *J. Power Sources*, **2015**, 294, 386–392.
10. Liu, Q.; Liu, L.; Xie, K.; Meng, Y.; Wu, H.; Wang, G.; Dai, Z.; Wei, Z.; Zhang, Z., Synergistic Effect of r-GO/PANI Nano composite Electrode based Air Working Ionic Actuator with Large Actuation Stroke and Long-Term Durability, *J. Mater. Chem. A*, **2015**, 3, 8380–8388.
11. Viri, S.; Kaner, R.R.B.; Weiller, B.H., Polyaniline nanofibers: facile synthesis and chemical sensors, *J. Phys. Chem. B*, **2006**, 110, 22266.
12. Li, W.; Jang, D.M.; An, S.Y.; Kim, D.; Hong, S.K.; Kim, H., Polyaniline-chitosan nanocomposite: High performance hydrogen sensor from new principle. *Sens. Actuators, B*, **2011**, 160, 1020–1025.
13. Hua, M.Y.; Lin, Y.C.; Tsai, R.Y.; Chen, H.C.; Liu, Y.C., A hydrogen peroxide sensor based on a horseradish peroxidase/polyaniline/carboxy-functionalized multi-walled carbon nanotube modified gold electrode, *Electrochim. Acta*, **2011**, 56, 9488.
14. Chen, X.; Chen, Z.; Zhu, J.; Xu, C.; Yan, W.; Yao, C., A novel H_2O_2 amperometric biosensor based on gold nanoparticles/self-doped polyaniline nanofiber, *Bioelectrochemistry*, **2011**, 82, 87.
15. A. Rydosz, Sensors for Enhanced Detection of Acetone as a Potential Tool for Noninvasive Diabetes Monitoring, *Sensors*, **2018**, 18, 2298.
16. S. K. Shukla, C. S. Kushwaha, and N. B. Singh, Recent developments in conducting polymer-based composites for sensing devices, *Mater. Today. Proc.*, **2017**, 4, 5672–5681.

 doi:10.20944/preprints202507.0811.v1

17. Kumar, L.; Rawal, I.; Kaur, A.; Annapoorni, S., Flexible room temperature ammonia sensor based on polyaniline, *Sens. Actuators B*, **2017**, 240, 408–416.
18. Qi, J.; Xu, X.; Liu, X.X.; Lau, K.T., Fabrication of textile based conductometric polyaniline gas sensor, *Sens. Actuators B*, **2014**, 202, 732–740.
19. Do, J. S.; Liu, W. L.; Tsai, M. L.; Kuo, S. Y., *Key Eng. Mater*., **2014**, 605, 202–206.
20. Zhang, D.; Wu, Z.; Zong, X., Flexible and highly sensitive H_2S gas sensor based on in-situ polymerized SnO_2/rGO/PANI ternary nanocomposite with application in halitosis diagnosis, *Sens. Actuators B*, **2019**, 288, 232–242.
21. Kim, J.S.; Byeon, J.H.; Kang, S.; Kim, J.Y., A high sensitivity acetone gas sensor based on polyaniline–hydroxypropyl methylcellulose core shell-shaped nanoparticles, *Nanoscale Adv*. **2022**, 4, 5312–5319.
22. Do, J. S.; Wang, S. H., On the sensitivity of conductimetric acetone gas sensor based on polypyrrole and polyaniline conducting polymers, *Sens. Actuators B*, **2013**, 185, 39–46.
23. Jun, H. K.; Hoh, Y. S.; Lee, B. S.; Lee, S. T.; Lim, J. O.; Lee, D. D.; Huh, J. S., Electrical properties of polypyrrole gas sensors fabricated under various pretreatment conditions, *Sens. Actuators B*, **2003**, 96, 576–581.
24. Drelinkiewicz, A.; Hasik, M.; Choczynski, M., Preparation and Properties of Polyaniline Containing Palladium, *Mater, Res. Bull.*, **1993**, 33, 739.
25. Ho, K.S.; Hsieh, T.H.; Kuo, C.W.; Lee, S.W.; Lin, J.J.; Huang. Y.J., Effect of aniline formaldehyde resin on the conjugation length and structure of doped polyaniline: Spectral studies, *J. Polym. Sci. Part A: Polym. Chem*., **2005**, 43, 3116.
26. Babu, V. J.; Vempati, S.; Ramakrishna, S., Conducting Polyaniline-Electrical Charge Transportation, *J. Sci. Res*., **2013**, 4, 1–10.
27. Srinivasan, P.; Gottam, R., Infrared Spectra: Useful Technique to Identify the Conductivity Level of Emeraldine form of Polyaniline and Indication of Conductivity Measurement either Two or Four Probe Technique, *Mat. Sci. Res. India*, **2018**, 15, 209–217.
28. Jang, J.; Cho, J.; Jang, J., Fabrication of Water-Dispersible Polyaniline-Poly(4-styrenesulfonate) Nanoparticles for Inkjet-Printed Chemical-Sensor Applications, *Adv. Mater*., **2007**, 19, 1772.
29. Hatchett, D.W.; Josowicz, M.; Janata, J., Acid Doping of Polyaniline: Spectroscopic and Electrochemical Studies, *J. Phys. Chem. B*, **1999**, 103, 10992.
30. Fu, Y.; Elsenbaumer, L., Thermochemistry and Kinetics of Chemical Polymerization of Aniline Determined by Solution Calorimetry, *Chem. Mater*., **1994**, 6, 671.
31. Jang, J. S.; Choi, S. J.; Kim, S. J.; Hakim, M.; Kim, I. D., Rational Design of Highly Porous SnO_2 Nanotubes Functionalized with Biomimetic Nanocatalysts for Direct Observation of Simulated Diabetes, *Adv. Funct. Mater*., **2016**, 26, 4740–4748.
32. Parkes, J. L.; Slatin, S. L.; Pardo, S.; Ginsberg, B. H. A., New Consensus error grid to evaluate the clinical significance of inaccuracies in the measurement of blood glucose, *Diabetes Care*, **2000**, 23, 1143–1148.
33. Turner, C.; Walton, C. C.; Hoashi, S.; Evans, M., Breath acetone concentration decreases with blood glucose concentration in type I diabetes mellitus patients during hypoglycaemic clamps, *J. Breath Res*., **2009**, 3, 046004.
34. Jaegle, L.; Jacob, D.J.; Brune, W.H.; Faloona, I.; Tan, D.; Heikes, B.G.; Kondo, Y.; Sachse, G.W.; Anderson, B.; Shetter, R.E. Photochemistry of Hox in the upper troposphere at northern midlatitudes. J. Geophys. Res. Atmos. **2000**, 105, 3877-3892.
35. Cyran, J.D.; Backus, E.H.G.; van Zadel, M-J.; Bonn, M. Comparative adsorption of acetone on water and ice surfaces, Angew. Chem. Int Ed. **2019**, 58, 3620-3624.